Molecular Neurobiology (2019) 56:2670–2684
https://doi.org/10.1007/s12035-018-1259-6

Dp71-Dystrophin Deficiency Alters Prefrontal Cortex Excitation-Inhibition Balance and Executive Functions

Rémi Chaussenot[1] · Muriel Amar[1,2] · Philippe Fossier[1] · Cyrille Vaillend[1]

Received: 19 April 2018 / Accepted: 17 July 2018 / Published online: 27 July 2018

Abstract

In the Duchenne muscular dystrophy (DMD) syndrome, mutations affecting expression of Dp71, the main dystrophin isoform of the multipromoter *dmd* gene in brain, have been associated with intellectual disability and neuropsychiatric disturbances. Patients' profile suggests alterations in prefrontal cortex-dependent executive processes, but the specific dysfunctions due to Dp71 deficiency are unclear. Dp71 is involved in brain ion homeostasis, and its deficiency is expected to increase neuronal excitability, which might compromise the integrity of neuronal networks undertaking high-order cognitive functions. Here, we used electrophysiological (patch clamp) and behavioral techniques in a transgenic mouse that display a selective loss of Dp71 and no muscular dystrophy, to identify changes in prefrontal cortex excitatory/inhibitory (E/I) balance and putative executive dysfunctions. We found prefrontal cortex E/I balance is shifted toward enhanced excitation in Dp71-null mice. This is associated with a selective alteration of AMPA receptor-mediated glutamatergic transmission and reduced synaptic plasticity, while inhibitory transmission is unaffected. Moreover, Dp71-null mice display deficits in cognitive processes that depend on prefrontal cortex integrity, such as cognitive flexibility and sensitivity of spatial working memory to proactive interference. Our data suggest that impaired cortical E/I balance and executive dysfunctions contribute to the intellectual and behavioral disturbances associated with Dp71 deficiency in DMD, in line with current neurobehavioral models considering these functions as key pathophysiological factors in various neurodevelopmental disorders. These new insights in DMD neurobiology also suggest new directions for therapeutic developments targeting excitatory neurotransmission, as well as for guidance of academic environment in severely affected DMD children.

Keywords Glia · Mouse models · Intellectual disability · Cortical network plasticity · Working memory · Cognitive flexibility

Introduction

Cognitive deficits and comorbid diagnosis of neuropsychiatric disorders are well-recognized features of the Duchenne muscular dystrophy (DMD) syndrome, a common X-linked neuromuscular disorder caused by mutations in the dystrophin gene. The severity of central dysfunctions increases with mutations at the 3′ end of the gene, which lead to cumulative loss of several dystrophin-gene products (Dp260, Dp140, Dp116, and Dp71) encoded by distinct internal promoters and normally expressed in the nervous system in a cell-specific manner [1–4]. Although the molecular basis of the cognitive impairment is still poorly understood, phenotype-genotype relationships suggest that genetic loss of all dystrophin products is associated with severe intellectual disability (ID) and that Dp71 loss is a pivotal aggravating factor for cognitive status [5, 6]. This has been further supported by identification of the first mutation that selectively alters Dp71 function and results in ID without muscular dystrophy [7]. However, the respective roles of brain dystrophins in distinct cognitive functions and the core endophenotypes and neural mechanisms that lead to ID in DMD patients are still unclear.

While a range of cognitive and behavioral disturbances has been reported in heterogeneous cohorts of DMD

Rémi Chaussenot and Muriel Amar contributed equally to this work.

Electronic supplementary material The online version of this article (https://doi.org/10.1007/s12035-018-1259-6) contains supplementary material, which is available to authorized users.

✉ Cyrille Vaillend
cyrille.vaillend@u-psud.fr

[1] Neuroscience Paris-Saclay Institute (Neuro-PSI), UMR 9197, Université Paris Sud, CNRS, Université Paris Saclay, Orsay, France

[2] Laboratoire de Toxinologie moléculaire et Biotechnologies, Institut des Sciences du Vivant Frédéric Joliot, CEA de Saclay, 91191 Gif-sur-Yvette, France

patients ([8] for a review), dysfunction of high-order cognitive and executive processing, such as working memory, inhibition, and problem solving, is a general finding likely central for their general intellectual functioning [8, 9]. A recent study suggested that mutations affecting Dp71 in a subset of patients are preferentially associated with working memory deficits and presence of neuropsychiatric disorders as compared to more proximal mutations in the *dmd* gene [10]. The prefrontal cortex is a key brain structure involved in undertaking executive functions in mammals [11, 12]. Accordingly, neurodevelopmental disorders such as autism, schizophrenia, and intellectual disability, which frequently come along with working memory, executive function, and social deficits, have been associated with prefrontal cortex dysfunction with altered tuning of cortical excitatory/inhibitory (E/I) balance [13–15]. However, no study had specifically addressed such prefrontal cortex functions in animal models of DMD.

Dp71 is the shortest but most abundantly expressed dystrophin-gene product in the brain [16]. In common with the other non-muscle dystrophins, Dp71 contains the cysteine rich and carboxy-terminus domains of dystrophin, which are required for binding to transmembrane dystroglycan and adapter-protein syntrophin involved in the membrane clustering of various ion channels and receptors [17]. Dp71 is enriched in perivascular-astrocyte endfeet throughout the brain, where it is required for proper localization of AQP4 and Kir4.1 channels [18]. It has been hypothesized that Dp71 loss might thus alter both water and potassium homeostasis and perhaps enhance neuronal excitability [19]. A pool of Dp71 is also expressed in postsynaptic densities, and we previously showed that Dp71 loss in mice induces learning and memory deficits and a disorganization of postsynaptic molecular scaffolds in glutamatergic synapses [20, 21]. Therefore, both glial and neuronal changes due to Dp71 loss have the potential to alter the E/I balance in neuronal networks involved in undertaking high-order cognitive and executive functions.

To address this hypothesis, we characterized the neurophysiological mechanisms and behavioral processes associated with executive functioning in Dp71-null mice, which have a selective inactivation of the Dp71 promoter and do not display muscular dystrophy. We used patch-clamp techniques in acute medial prefrontal cortex (mPFC) slices to show that key brain mechanisms involved in prefrontal cortex functions, such the basal set-point value of E/I balance, glutamatergic transmission, and synaptic plasticity, are drastically altered in Dp71-null mice. By means of specific behavioral paradigms, we further show that executive functions that rely on integrity of prefrontal cortex, such as spatial working memory and cognitive flexibility, are also compromised in these mice.

Materials and Methods

Animals

Dp71-null mice were originally generated by homologous recombination by replacing most of the first and unique exon and a small part of the first intron of Dp71 by the promoterless gene encoding a β-gal-neomycin resistance chimeric protein, which specifically abolishes the transcription of Dp71 mRNA without interfering with the expression of other *dmd*-gene products [22]. Transgenic mice were backcrossed for > ten generations to C57BL/6JRj mice (Janvier Labs, France) in CDTA (Orléans, France), and breeders were kindly provided by Dr. Alvaro Rendon (Institut de la Vision, Paris, France). Production and maintenance of the transgenic line were undertaken in our animal facility by crossing heterozygous females with C57BL/6JRj males to generate Dp71 null and littermate control (WT) male mice. Genotype was determined by detecting presence of the gene encoding β-gal in PCR analyses of tail DNA. Animals were kept under a 12-h light-dark cycle (light on 7 a.m.) with food and water ad libitum. Independent groups of 10–16 weeks male siblings were used for behavioral testing; test mice were placed in individual caging for at least 8 days before testing, and most protocols were conducted as previously described [23]. Studies were conducted blind to the genotype.

Semi-Quantitative Immunofluorescence and Confocal Image Analyses

Brains dissected out following cervical dislocation were fresh frozen in powdered dry ice and stored at −80 °C. Coronal brains sections (30 μm thick) including the mPFC were cut at −12 °C in a cryostat and collected on Superfrost Plus glass slides (Roth, France). For immunochemistry, slides were thawed for 1 min at RT, immersed in acetone/methanol (1:1) for 5 min at −20 °C, washed three times in 0.1 M phosphate-buffered saline (PBS), incubated in a blocking solution for 45 min (10% normal goat serum, 0.3% Triton X-100, 1% bovine serum albumin) and then overnight at 4 °C with a primary polyclonal antibody directed against the postsynaptic density protein PSD-95 (1:500, Invitrogen). Sections were then washed and incubated with a goat anti-rabbit secondary antibody conjugated to Cy3 (Jackson ImmunoResearch, USA) diluted 1:500 in PBS 0.1 M with 5% NGS and 1% BSA for 1 h at RT. Slides were then washed and coverslipped using a mounting medium containing an instant-blue nuclear probe fluorescing (455 nm) compound (DAPI Fluoromount-G, Clinisciences, France). No staining was observed in sections processed from control sections from both genotypes, when primary antibody was omitted.

A laser scanning confocal microscope LSM 700 (Zeiss) was used to sequentially collect Cy3 immunoreactivity at 555 nm

and DAPI staining at 405 nm. Confocal images of mPFC were imported using an EC Plan-Neofluar 40x/1.30 Oil M27 at a resolution of 156 nm/pixel. All images were randomly taken in layers 2/3 at same exposure times and equivalent stereotaxic coordinates (bregma 2.8 mm to 2.46 mm; mouse brain atlas; [24]). Images were processed for quantification using the WCIF ImageJ imaging system as follows: the punctate IR representing presumptive protein clusters, with a minimal size of clusters arbitrarily set to three adjacent pixels (0.05 μm^2) and a maximal size of 1 μm^2, corresponding to more than 99% of the counted clusters. A threshold segmentation algorithm was used for automatic detection of clusters [25]. The number and size of the clusters were analyzed within a total tissue surface of 43,200 μm^2 per genotype derived from four brain sections per animal. The Kolmogorov-Smirnov test (KS-test) was used to compare the distribution of protein cluster sizes.

Electrophysiology

Whole-Cell Patch-Clamp Recordings

Coronal brain slices (250 μm thick) including the mPFC were obtained at postnatal days 21–28 (P21-P28) and maintained at 33 °C in an oxygenated (95% O_2–5% CO_2) artificial cerebrospinal extracellular solution (ACSF) containing (in mM): 126 NaCl, 26 $NaHCO_3$, 10 Glucose, 2 $CaCl_2$, 1.5 KCl, 1.5 $MgSO_4$, and 1.25 KH_2PO_4 (pH 7.5, 310–330 mOsm). Somatic whole-cell voltage-clamp and current-clamp recordings were obtained with a MultiClamp 700B amplifier (Axon Instruments, USA) from layer 5 pyramidal neurons identified from the shape of their soma and primary dendrites using video-enhanced DIC (Hamamatsu Photonics, Japan) and from their current-induced firing profile. The borosilicate glass pipettes (3–5 MΩ) were filled with (in mM) 140 K-gluconate, 10 HEPES, 4 ATP, 2 $MgCl_2$, 0.4 GTP, and 0.5 EGTA (pH 7.3 adjusted with KOH, 270–290 mOsm). Signals were filtered at 2 kHz by a low-pass Bessel filter and sampled at 4 kHz using a National Instruments BNC-2090A acquisition board. Voltage data were corrected off-line for a measured liquid junction potential of − 10 mV. The membrane time constant (τ) of each cell was determined from a voltage response induced by 50 pA hyperpolarizing steps (200 ms; repeated 12 times). Only cells with a resting potential of ≤ − 60 mV and an access resistance of < 25 MΩ were kept for analysis. The access resistance was compensated off-line in voltage-clamp mode, and neurons exhibiting more than 10% of the access resistance during the experiment were rejected. Electrical stimulations (1–10 μA, 0.2 ms) were delivered within layers 2/3 of mPFC using a 1 MΩ impedance bipolar tungsten stimulating electrode (TST33A10KT, WPI, Hertfordshire, England). The stimulation intensity was adjusted in current-clamp conditions to induce a subthreshold postsynaptic response reflecting coactivation of excitatory and inhibitory circuits without recruiting dominant non-linear processes such as those induced by NMDA receptor (NMDAr) activation. Control experiments with the NMDAr blocker D-AP5 did not reveal any variation of the recorded responses. Responses with antidromic spikes were discarded. In voltage-clamp conditions, the frequency of stimulation was 0.05 Hz, and five to eight responses were averaged for each holding potential. Control recordings were made after 15 min of patch-clamp equilibration at 0.05 Hz at 5–7 holding potentials around neuron resting potential and after 20 min of continuous drug perfusion. NBQX and D-AP5 were obtained from Ascent Scientific (Bristol, UK), spermine tetrahydrochloride, QX314, picrotoxin, and TTX from Tocris (R&D Systems, France). All other drugs and chemicals were obtained from Sigma-Aldrich (Lyon, France).

Data were analyzed off-line with a specialized software (Elphy™) developed by Sadoc G. at the Biologic UNIC–CNRS (Gif-sur-Yvette, France). The method is based on the continuous measurement of conductance dynamics during stimulus-evoked synaptic response, as primary described in vivo in the cat cortex [26, 27] and further validated in the rat visual cortex [28] and mouse mPFC [29, 30]. Evoked synaptic currents measured and averaged at a given holding potential were used to construct I-V curves. The holding potential value (Vh) was corrected (Vhc) to account for the resistance drop due to current leakage through resistance series (Rs) by the equation: $Vhc(t) = Vh(t) – I(t) \times Rs$. An average estimate of the cell input conductance waveform was calculated from the best linear fit (mean least square criterion) of the I-V curve for each delay (t) following stimulation onset. Cells showing a Pearson correlation > 0.95 with the I-V linear regression slope between − 90 and − 40 mV were used to calculate the conductance change in the recorded pyramidal neuron from the slope of the linear regression.

Excitatory/Inhibitory (E/I) Balance

Somatic recordings do not provide rigorous estimates of the synaptic events in distal dendrites and the conductance estimates are ratios of the overall excitatory and inhibitory drive contained in the stimulated local network [31]. However, relative changes in conductance magnitude reflect the cumulative contributions of excitation and inhibition that converge at proximal portions of the neuron and define a narrow window over which input integration and spike output can occur [32]. Therefore, we estimated the E/I balance through the decomposition of synaptic conductance changes as described [27–30]. The evoked synaptic global conductance term $gT(t)$ was first calculated by subtracting the resting conductance (g_{rest}) from input conductance. The apparent reversal potential of the synaptic conductance at the soma ($Esyn(t)$) was taken as the voltage abscissa of the intersection point between the I-V curve obtained at a given time (t) and that determined at rest. Assuming that the evoked somatic conductance change

reflects the composite synaptic input reaching the soma, Esyn(t) characterizes the stimulation-locked dynamics of the excitation/inhibition balance.

To decompose the global evoked synaptic conductance (gT(t)) into excitatory and inhibitory components (gE(t) and gI(t)), each was associated with known and fixed reversal potentials. The following simplification was used: Isyn(t) = gE(t) (Esyn(t)–Eexc) + gI(t) (Esyn(t)–Einh) and gT(t) = gE(t) + gI(t), where Isyn(t) is the total synaptic current, Esyn(t) is the apparent reversal potential at the soma, gE(t) and gI(t) are excitatory and inhibitory conductances respectively, and Eexc and Einh are the reversal potentials for excitation and inhibition currents (program written by C. Monier, CNRS UNIC, France). The I-V curve in layer 5 of the mPFC was linear between − 80 to + 10 mV with a reversal potential equal to − 80 mV in the presence of excitatory transmission blockers (CNQX, D-AP5) and to 0 mV in the presence of the bicuculline blocker of inhibitory inputs [30]. Esyn(t) was extrapolated from I-V curves in which it took any intermediate values between − 80 mV and − 40 mV ([30] in supplementary data), i.e., within the limits of the voltage range (− 90 to − 40 mV) corresponding to the linear part of I-V curves. Esyn(t) was also within the limits of Einh and Eexc values, in order to fulfill mathematical conditions for simplification of the gI(t) and gE(t) calculation. Synaptic conductance changes were quantified as integrals (int) within a 200 ms time window, to reach a better reproducibility than with direct measurement of peak conductance. The contribution of each component of the E/I balance was expressed by the ratio of its integral values (IntgE or IntgI) and the global conductance change (IntgT).

Synaptic Transmission

Synaptic efficacy was first evaluated by means of input/output (I/O) curves generated using a range of stimulus intensities from 0 to 40 V. Four responses were averaged at each intensity. NMDAr-mediated synaptic responses were isolated in the presence of a $GABA_A$ receptor antagonist (picrotoxin, 50 μM) and an AMPA receptor antagonist NBQX, 10 μM) at a holding potential of − 40 mV. NMDAr activation was confirmed by applying an NMDAr antagonist (D-AP5, 50 μM). To estimate the NMDA/AMPA ratio, the recording pipettes were filled with (in mM) 115 $NaCH_3CsSO_3$, 20 CsCl, 10 HEPES, 2.5 $MgCl_2$, 4 Na_2ATP, 0.4 NaGTP, 10 Na-p-creatinine, 0.6 EGTA, 0.1 spermine tetrahydrochloride, and 5 QX314 (280–300 mOsm, pH 7.3 adjusted with CsCL OH). Pyramidal neurons in layer 5 were clamped at − 75 mV and AMPAr-mediated EPSCs were recorded in response to single pulses delivered at 0.05 Hz in layer 2/3. NBQX (10 μM) was then applied to ACSF and the holding potential changed to + 40 mV to isolate NMDAr-mediated EPSCs. Picrotoxin (50 μM) was present to block $GABA_A$ receptor-mediated currents.

Spontaneous miniature excitatory postsynaptic currents (mEPSC) were recorded at − 75 mV in whole-cell configuration in the presence of bath-applied sodium channel blocker tetrodotoxin (TTX, 1 μM), D-AP5 (50 μM), and picrotoxin (50 μM). NBQX (10 μM) suppressed mEPSCs thus confirming their dependence on AMPAr activation. Spontaneous miniature inhibitory postsynaptic currents (mIPSC) were recorded at a holding potential of − 75 mV and a Cl^- reversal potential around − 35 mV, in the presence of bath-applied TTX (1 μM), NBQX (10 μM), and D-AP5 (50 μM). Picrotoxin (50 μM) suppressed mIPSCs thus confirming their dependence on $GABA_A$r activation. The amplitude and frequency of at least 300 mEPSCs and 300 mIPSCs were analyzed with the Elphy software.

Synaptic Plasticity

Paired-pulse facilitation (PPF) of evoked EPSCs was examined at varying interstimulus intervals (ISI from 50 to 700 ms), using a stimulation intensity corresponding to one third of the intensity necessary to elicit an action potential. Four responses were averaged for each ISI. Long-term synaptic plasticity was induced in prefrontal cortical layer 2/3 by high-frequency stimulation (HFS) using a theta burst protocol (three trains of 13 bursts at 5 Hz, each burst comprising four pulses at 100 Hz; 2 min total duration), while layer 5 neurons being under current clamp ($I = 0$) [33]. Data were recorded 15, 30, 45, and 60 min after HFS and compared to baseline recordings. Synaptic plasticity was considered when the induced changes in synaptic strength were larger than 20% of baseline recordings.

Behavioral Studies

Auditory Gating

The conditioning chamber (19 × 25 × 19 cm) was placed inside a sound-attenuating box (67 × 53 × 55 cm, StartFear System, Panlab, Spain) and was composed of black methacrylate walls, a transparent front door, a roof speaker, and a grid floor (StartFear System, Panlab). Mice were placed on the grid floor in a small non-restraining plexiglas cylinder (5 × 10 × 3.5 cm) during 5 min prior to testing (acclimation period). A background white noise (BWN, 65 dB) was present throughout testing. The acoustic startle reflex (ASR) was induced by a high-intensity startling tone (pulse; 55 dB above background noise, 10 kHz, 40 ms), and its amplitude was modulated by the presentation of non-startling low-intensity prepulses (0–12 dB above background noise, 10 kHz, 20 ms) to evaluate auditory gating. Startle responses were detected by a piezoelectric accelerometer plugged to the grid floor. The startle reflex was first evaluated by exposing mice to four blocks of nine pulses (5, 15, 25, 30, 35, 40, 45, 50, 55 dB above BWN) presented in a pseudorandom order with intertrial intervals (ITIs) of 10, 15,

or 20 s. On the next day, the capacity of a prepulse to reduce the amplitude of the startle reflex (prepulse inhibition of ASR, or PPI) was evaluated by exposing mice to six blocks of five pairs of stimuli, each composed of one prepulse (0, 3, 6, 9, or 12 dB above BWN) delivered 100 ms before a startling pulse of 120 dB (55 dB above BWN).

Navigation and Reversal Learning in the Water Maze

The maze was a circular tank (150 cm in diameter) filled with water (21–22 °C) to 7 cm below the top of the sidewall, made opaque by addition of a white non-toxic paint (Opacifier 631, Morton SA, France). A circular escape platform (11 cm in diameter) was placed in the center of the maze during pretraining or in the center of a quadrant (40 cm from the wall) during training. The platform placed 0.5 cm below, the water surface was not visible. The maze was placed in a well-lit room (380 lx) containing several extramaze cues. A video camera mounted on the ceiling was connected to a computer in an adjacent room, and data were recorded using the AnyMaze Video Tracking System (Stoelting, USA). One day before training, the mice underwent four trials during which they were trained to find and stay on the escape platform for 60 s (pretraining). Then, the training phase lasted 9 days and consisted of four successive trials during which the platform was always located in the same quadrant for a given mouse. In each trial, the mouse was introduced in the water maze from three different starting points in the quadrants that did not contain the platform and was allowed to swim freely until it reached the platform. Mice failing to find the platform after 90 s were gently guided to it by hand, and a maximum escape latency of 90 s was recorded. Mice remained 60 s on the platform before the start of the next trial. After the training phase, the platform was moved in the opposite quadrant and mice were given five additional days of training to learn the new platform position (reversal). Individual swim paths were recorded to calculate swim speed, distance swum, and time spent in various virtual areas of the maze: The four quadrants, the four platform annuli representing putative platform positions, four extended annuli (48 cm in diameter) surrounding platform positions, and a virtual corridor 19 cm in width set along the wall to quantify thigmotaxis. Path efficiency was defined as an index of the path taken by the animal to get from its start position to the platform, with a score of 1 indicating perfect efficiency (straight-line trajectory).

Reversal Learning and Working Memory in the Radial Maze

The automated radial maze (Ugo Basile, Italy) had a central platform (16 cm in diameter) and eight arms (5.5 × 35 cm) with low-profile walls (height, 1 cm; initial step from door, 8 × 7-cm length) to optimize visibility of extramaze cues for allocentric spatial orientation. A guillotine-like mechanism enabled to quickly but silently open and close individual sliding doors at the entrance of each arm. Independent groups of mice of both genotypes were submitted either to a win-stay learning paradigm to test reversal learning or to a win-shift paradigm to evaluate spatial working memory performance. Mice were first placed under a water restriction regimen with daily access to 0.2 ml of the solution to be used as the reward during training (reversal testing, 0.1% saccharine solution; DNMTP, sweetened condensed milk diluted 1:1 in water) followed by access to 1 ml of water. Mice were maintained at 85–90% of their initial weight throughout the experiment. Mice were given 1 ml drinking water in their home cage after each session.

For reversal testing, mice were first allowed to freely explore the maze with all doors opened for 2 days, during which they could retrieve three (on day 1) or one (on day 2) 15-μl drops of the reward solution in each arm (pretraining). Training then consisted in a 10-day training phase, during which mice had to retrieve one reward placed in a small cup at the end of one single baited arm, in six consecutive trials per day. Each trial started by placing mice on the central platform for 15 s before opening all doors and ended when the mouse reached the end of the baited arm and returned to the central platform after consuming the reinforcement, or after a maximum duration of 300 s. The baited arm was the same throughout this initial discrimination task for a given mouse. On day 11, the reward was moved to a new baited arm located 135° anticlockwise from the previously baited arm, and the mice had to learn the new rewarded position for 4 days (reversal learning). Mice were returned to their home cage for 60 s between each trial. Reference memory errors were defined as first visits into non-baited arms and working memory errors as revisits of non-baited arms within the same trial.

For working memory, we first used a low-interference paradigm. Training lasted 7 days and consisted of two trials per day (online resource; Fig. S5 a). Each trial started by placing the mouse on the central platform before door opening. During a presentation phase, only three doors were opened to provide access to only three baited arms. Mice were then maintained on the central platform for 15 s before start of a choice phase during which six doors were simultaneously opened, giving access to the three previously baited arms and to three novel arms. Only the three novel arms were baited during the choice phase. On day 8, working memory performance was challenged by increasing the delay between the presentation and choice phases to 30 s instead of 15 s.

In a second experiment, we analyzed working memory performance using a high-interference delayed non-matching to place task, or DNMTP. Testing started with a pretraining phase lasting 4 days during which the mice were given sequential access to each baited arm until the entire maze was visited within a single session. Then, DNMTP consisted of eight trials per day for 14 days. In each trial, the mouse could first sequentially visit two different baited arms (study phase).

After entering the last arm and returning to the central platform for 5 s, it was then submitted to a choice phase consisting in two trials (two choice pairs) during which it had the choice to visit a new arm, or an arm previously visited during the study phase. Only the new arm was baited, and a visit to this arm was counted as a correct choice. For each choice pair, once the mouse had made a choice, the door of the other open arm was closed. The mouse first had simultaneous access to the first arm previously visited during the study phase and a new adjacent baited arm (first choice). Then, it was given access to the second arm previously visited during the presentation phase and a new adjacent baited arm (second choice). The sequences of presented arms during the study and choice phases were pseudorandomly selected [34]. In each trial, the mouse was given a score equal to 100% if it only visited new baited arms during the choice phase, 50% if it visited one of the two new baited arms, and 0% if incorrect choices were made in both trials.

Statistical Analysis

For data expressed as means ± standard errors of the mean (SEMs), genotype differences were evaluated using one or two-way ANOVAs depending on the presence of a within-subject repeated measure (intensity, time, training session); p values < 0.05 were considered statistically significant. The Kolmogorov-Smirnov (K-S) test was used to analyze the cumulative distributions of frequency and amplitude of miniature currents in the patch-clamp study and of protein cluster size in confocal image analyses; p values < 0.005 were considered statistically significant.

Results

Neurophysiology of Prefrontal Cortex Pyramidal Neurons

Intrinsic Membrane Properties

Stable patch clamp of pyramidal neurons was obtained in layer 5 of medial prefrontal cortex (mPFC) in juvenile male mice of both genotypes (online resource; Fig. S1). Recordings displayed the typical intrinsic properties and firing patterns of regular spiking pyramidal neurons [35, 36]. As shown in online resource (Table S1), passive membrane properties characterized by membrane resting potential (Vm), input resistance (Ri), and time constant (τm) were statistically comparable between genotypes (all three parameters, $p > 0.1$, NS). The action potential (AP) threshold was slightly higher in Dp71-null mice compared to WT (≈ + 2 mV; $p < 0.05$), but this was not associated with significant changes in AP half width, dV ratio, and firing rate.

Excitatory Synapse Organization and Glutamatergic Transmission

Synaptic expression of the postsynaptic density protein, PSD-95, was characterized as punctate immunofluorescent dots of different sizes (clusters) scattered in dendritic areas of principal cells in mPFC cortical layers (Fig. 1a). There was a rightward shift of the distribution curves of PSD-95 cluster sizes in Dp71-null mice compared to WT mice (K-S test, $p < 0.005$), indicating a higher proportion of large protein clusters in Dp71-null mice.

Synaptic transmission in layer 5 neurons of mPFC was first evaluated by constructing input/output curves reflecting the proportional increase in the evoked EPSC amplitude with increasing stimulus intensity (Fig. 1b). EPSC amplitude was abnormally enhanced in Dp71-null mice at all stimulus intensities (7 cells; 4 mice) compared to WT littermate mice (10 cells; 4 mice) ($p = 0.024$). The genotype difference was readily observable from the lowest stimulation intensity, suggesting a main involvement of AMPA receptor-dependent transmission. To test this hypothesis, we further investigated the two main components of glutamatergic neurotransmission mediated by the AMPA/kaïnate and NMDA receptors (AMPAr, NMDAr) (Fig. 1c). Clamping the cell voltage at − 75 mV in the presence of the $GABA_A$-receptor antagonist picrotoxin (50 μM) enabled isolation of the fast AMPAr-mediated inward current, which could be abolished by the AMPAr antagonist NBQX (10 μM). Then, depolarizing the same cell to + 40 mV in the presence of picrotoxin and NBQX revealed a slower outward current that was blocked by the NMDAr antagonist D-AP5 (50 μM), which therefore corresponded to the NMDAr-mediated component of neurotransmission. The ratio of NMDAr and AMPAr-dependent peak amplitudes (NMDA/AMPA ratio) was significantly reduced in Dp71-null mice compared to WT mice (Dp71-null, 0.39 ± 0.05, $n = 14$ cells, 5 mice; WT, 0.63 ± 0.05, $n = 34$ cells, 8 mice; $p = 0.0135$; Fig. 1c). As shown in Fig. 1d, in a subgroup of cells in which NMDAr-mediated current amplitudes were closely comparable between genotypes, the AMPAr-mediated currents were significantly increased in cells from Dp71-null mice (702.8 ± 105 pA; $n = 5$ cells, 4 mice) compared to WT mice (385.45 ± 50.88 pA; $n = 11$ cells, 4 mice) ($p < 0.008$).

Presynaptic and Postsynaptic Components of Neurotransmission

Spontaneous miniature postsynaptic currents were studied to decipher putative alterations of presynaptic and postsynaptic mechanisms involved in quantal neurotransmission and to assess a possible reduction in inhibitory (GABAergic) transmission. The distribution of interevent intervals (frequency) and peak amplitudes of miniature EPSCs (mEPSCs; first 300 events; $n = 11$ cells per genotype) and mIPSCs (first 300

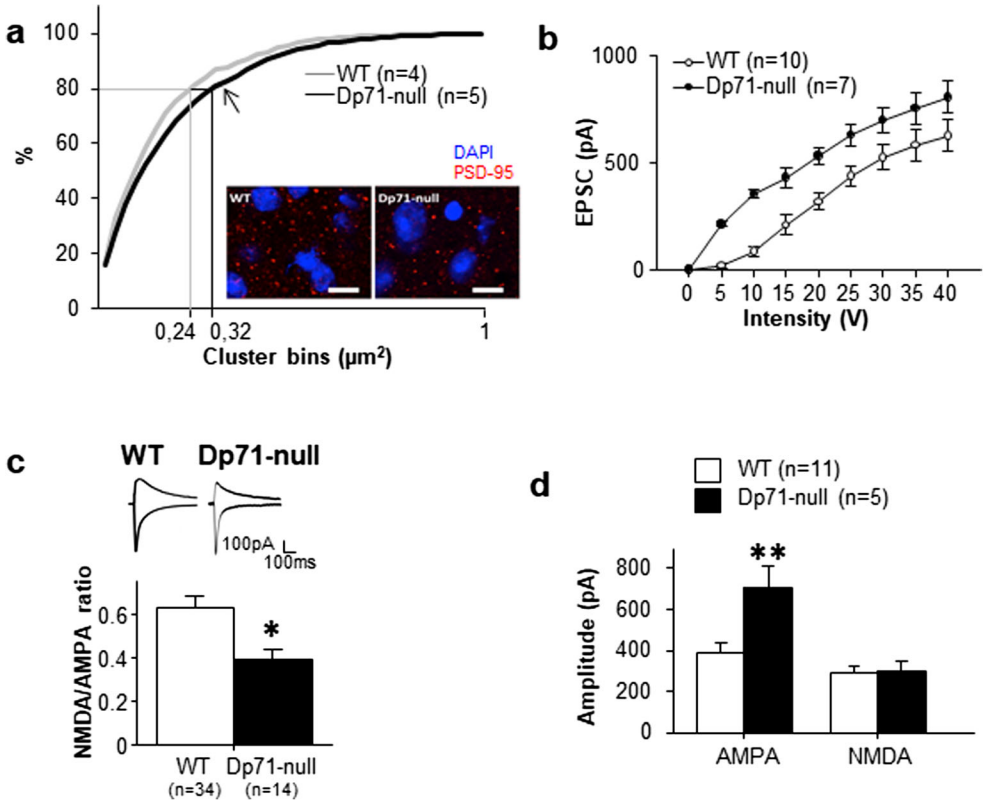

Fig. 1 Excitatory synapse organization and neurotransmission. **a** Immunoreactivity of PSD-95 in dendritic areas of mPFC. Cluster sizes were analyzed in a cumulative frequency curve. Inserts show raw sample confocal images of protein clusters (red) and neuron nuclei (blue) in each genotype. Scale bar, 10 µm. The distribution of PSD-95 clusters (0.05 to 1 µm^2) showed a rightward shift in Dp71-null mice (arrow), with 80% of clusters ≤ 0.24 µm^2 in WT mice ($n = 4$ mice) versus 80% ≤ 0.32 µm^2 in Dp71-null mice ($n = 5$ mice). **b** Input-output curve showing the amplitude of EPSCs recorded at a − 75 mV holding potential in layer 5 mPFC neurons following low-frequency subthreshold electrical stimulation in layer 2/3 at various intensities (7 cells in Dp71-null and 10 cells in WT mice). **c** Reduced NMDA/AMPA current ratio in Dp71-null mice (14 cells in Dp71-null and 34 cells in WT mice). Sample traces show AMPAr-mediated (downward trace) and NMDAr-mediated (upward trace) synaptic currents averaged from a series of 10 consecutive evoked EPSCs. **d** In a subset of neurons in which the NMDAr component of EPSCs was comparable between genotypes (5 cells in Dp71-null and 11 cells in WT mice), the amplitude of AMPAr-mediated currents was increased in Dp71-null mice compared to WT mice. *$p < 0.05$, **$p < 0.01$, genotype effect

events; $n = 25$ cells in Dp71-null mice and 20 cells in WT mice) were analyzed as cumulative plots normalized to maximal values (Fig. 2). The frequency of miniature events accounts for presynaptic mechanisms, while their amplitude reflects postsynaptic parameters. For mEPSCs frequency (Fig. 2b), there was a leftward shift of the cumulative plot toward smaller frequencies in Dp71-null mice ($p < 0.0001$), reflecting a lower probability of glutamate release in this transgenic model. However, there was a shift toward larger values in the distribution of peak amplitudes in Dp71-null mice ($p < 0.0001$; Fig. 2c), suggesting an increase in the sensitivity of their postsynaptic glutamate receptors. While the time to peak of mEPSCs was comparable between genotypes (WT: $\tau_{on} = 2.47 \pm 0.09$ ms; Dp71-null, $\tau_{on} = 2.59 \pm 0.05$ ms; $n > 100$ events in 6 cells in both genotypes; $p = 0.3133$), the decay time constant was significantly smaller in Dp71-null mice (WT: $\tau_{off} = 6.69 \pm 0.15$ ms; Dp71-null, $\tau_{off} = 5.6 \pm 0.16$ ms, $p < 0.0001$) (online resource; Fig. S2), suggesting a change in AMPAr properties and/or subunit composition. In contrast, the frequency and amplitude of mIPSCs were strictly comparable between genotypes (Fig. 2d-f), as well as mIPSCs kinetics ($p > 0.05$), thus indicating that GABAergic neurotransmission was unaltered in Dp71-null mice.

Excitatory/Inhibitory (E/I) Balance

The relative contribution of excitatory and inhibitory currents to cortical synaptic balance was extracted through decomposition of the composite synaptic response recorded in layer 5 pyramidal neurons, which enables better evaluation of evoked inputs reaching the soma of neurons. We first performed extraction of the evoked total input synaptic conductance gT (online resource; Fig. S3) followed by its decomposition to determine somatic excitatory gE and inhibitory gI input conductances (Fig. 3a-b).

Typically, electric stimulations in layer 2/3 produced a fast excitatory conductance followed by a long-lasting inhibitory conductance. Integrals of gE (IntgE) and gI (IntgI) calculated

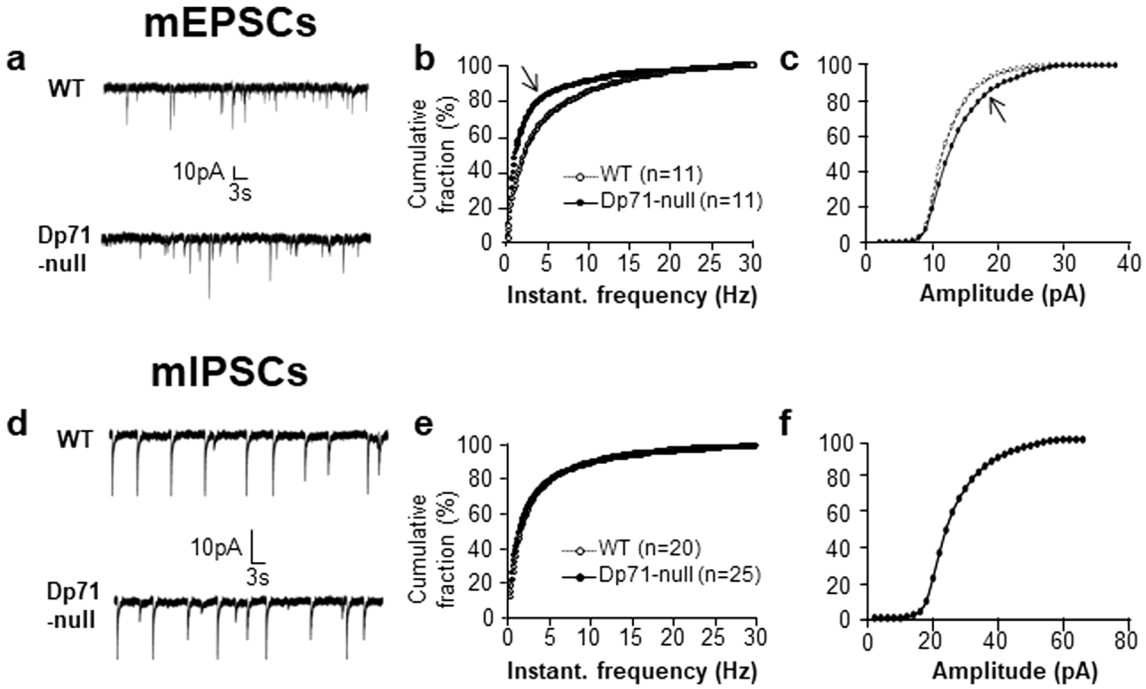

Fig. 2 Spontaneous miniature excitatory and inhibitory currents. **a** Representative traces of mEPSCs recorded at holding potential of − 75 mV in presence of TTX, D-AP5, and picrotoxin. **b–c** Cumulative fraction plots of instantaneous frequencies and peak amplitudes of mEPSCs (11 cells per genotype). Arrows show the leftward shift in frequencies and rightward shift in amplitudes in Dp71-null mice. **d** Representative traces of mIPSCs recorded at holding potential of − 75 mV in presence of TTX, D-AP5, and NBQX. **e–f** Cumulative fraction plots of instantaneous frequencies and peak amplitudes of mIPSCs (25 cells in Dp71-null and 20 cells in WT mice)

were then expressed as percentage of the total conductance integral (IntgT) to represent the E/I balance. The E/I ratio was significantly altered in Dp71-null mice ($n = 33$ cells in 12 mice) compared to WT littermate mice ($n = 29$ cells in 12 animals). The WT mice exhibited 18% excitation and 82% inhibition; whereas, the E/I balance was clearly skewed toward enhanced excitation in Dp71-null mice (26%/74%) ($p = 0.031$; Fig. 3c). The E/I ratio was therefore significantly increased in Dp71-null mice (ratio = 0.33) compared to WT mice (ratio = 0.225) ($p = 0.0042$; Fig. 3d).

Synaptic Plasticity

Short-term presynaptic facilitation of neurotransmission [37, 38] was tested by stimulating at subthreshold intensities in layer 2/3 with paired pulses with variable interstimulus intervals (ISI) (online resource; Fig. S4). Paired-pulse facilitation (PPF) of EPSCs observed in both genotypes was maximal at the shortest delay (50 ms) and decreased to baseline at longer ISIs. There was no statistical difference between genotypes.

Long-term synaptic plasticity was induced by a theta burst protocol (TBS) and expressed as the percentage change in the integral total conductance (IntgT) compared to baseline. In WT mice, TBS resulted in the induction of a long-term potentiation of synaptic transmission (LTP) characterized by a strong and lasting potentiation of the composite synaptic response (Fig. 3e), with a comparable potentiation of both excitation and inhibition (Fig. 3f, g, respectively). In Dp71-null mice, the potentiation of the composite response was significantly reduced compared to WT mice (Dp71-null, 43 ± 3.9%, $n = 21$ cells; WT, 67 ± 4.6%, $n = 13$ cells; $p = 0.00046$; Fig. 3d). This was associated with a reduced potentiation of the excitatory component (IntgE) in Dp71-null mice (only + 27%) compared to WT mice (+ 68%) ($p = 0.0006$; Fig. 3g). In contrast, the potentiation of the inhibitory component (IntgI) was comparable between genotypes ($p = 0.1$, NS; Fig. 3f). When LTP was induced after having pharmacologically isolated AMPAr-mediated EPSCs (Fig. 3h), the expression of AMPAr-mediated LTP was altered in the Dp71-null mice (genotype × time interaction, $p < 0.003$), with a reduced magnitude as compared to WT mice 60 min after LTP induction ($p < 0.04$).

Sensory Processing and Executive Functions

Sensory Gating

The capacity to integrate and gate auditory stimuli was addressed using a paradigm based on inhibition of the startle reflex. We first quantified the amplitude of the startle reflex elicited by increasing pulse intensities (Fig. 4a) and found no significant difference between genotypes (genotype, $p > 0.1$, genotype × intensity interaction, $p > 0.1$). Latencies of startle responses were also unaffected (genotype, $p > 0.7$, genotype ×

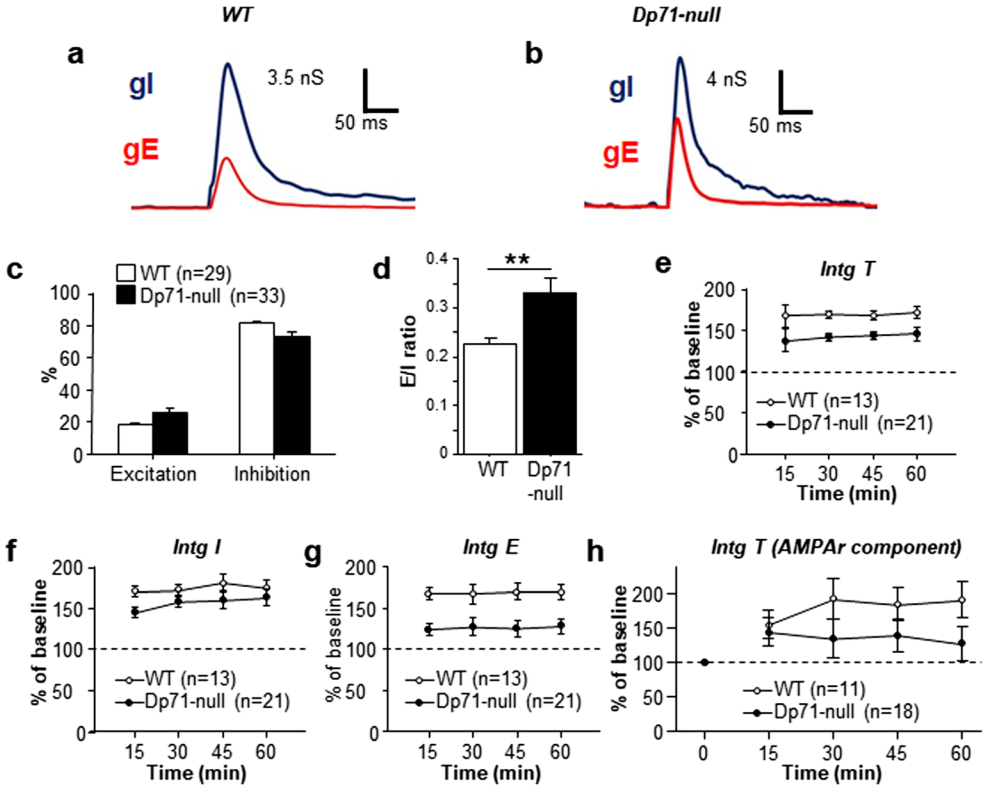

Fig. 3 Excitatory/inhibitory (E/I) balance and synaptic plasticity in mPFC neurons. The number of cells per genotype (*n*) is indicated in figure parts showing quantitative values. **a–b** Sample traces from WT (**a**) and Dp71-null mice (**b**) showing somatic excitatory (gE, red line) and inhibitory (gI, dark blue line) input conductances extracted by decomposition. **c** Percentage of excitation and inhibition diverged between genotype, with a shift toward enhanced excitation in Dp71-null mice. Synaptic conductance changes were evaluated by the ratio of their integral values (IntgE or IntgI) to that of global conductance changes (IntgT, online resource; Fig. S3). **d** Histogram showing the consequent enhancement of the E/I ratio in Dp71-null mice. $*p < 0.01$, genotype effect (same cells as in Fig. 3c). **e–g** Long-term potentiation (LTP) of synaptic transmission was characterized by an increase in total integrated conductance Intg T (**e**) with overt potentiation of both inhibitory IntgI (**f**) and excitatory IntgE (**g**) components of this composite total conductance. LTP of IntgT and IntgE was significantly reduced in Dp71-null mice, while the level of potentiation of inhibitory inputs was comparable between genotypes. **h** LTP of AMPAr-dependent EPSCs was lower in Dp71-null mice

intensity interaction, $p > 0.7$), confirming unimpaired startle reflex in Dp71-null mice. Moreover, the 120-dB pulses (55 dB above background) presented at the beginning (priming) and end (ending) of experiment elicited comparable responses in both genotypes ($p > 0.3$; Fig. 4a), indicating that the maximal startle response does not show notable variation over the course of an experiment. In a second experiment, a non-startling prepulse (3–12 dB above background noise) was delivered 100 ms before the 120 dB startling pulse (Fig. 4b). This induced a progressive decrease in startle amplitude as a function of prepulse intensity ($p < 0.001$), i.e., a prepulse-induced inhibition (PPI) of the startle response. PPI was comparable between genotypes at all prepulse intensities ($p > 0.8$), showing that auditory sensory gating was unimpaired in Dp71-null mice.

Spatial Cognitive Flexibility

Mice were first trained in a spatial reference memory task followed by reversal learning in a water maze (Fig. 5a–b). During the first 8 days of training, Dp71-null mice swam longer distances (Fig. 5a) and displayed longer latencies to reach the platform and escape from water compared to WT mice (both parameters, $p < 0.05$). This was associated with reduced path efficiency in Dp71-null mice ($p < 0.05$; Fig. 5b). However, there was no main genotype effect on swim speed or thigmotaxis (both parameters, $p > 0.1$), suggesting that the altered progression of learning performance in Dp71-null mice was not influenced by non-cognitive factors. Upon reversal on day 10 (platform position change), WT mice showed a drop in performance characterized by a longer distance swum to platform and decreased path efficiency as compared to the last day of training. During the next 3 days, there was a progressive decrease in the distance swum to reach the new platform position ($p < 0.02$; Fig. 5a) and in the number of entries into the quadrant that previously contained the platform ($p < 0.01$). Within the 4 days of reversal the performance reflected by these parameters returned to levels comparable with those expressed at the end of initial training, showing that WT mice flexibly learned the new platform position. However, a significant genotype x session interaction was detected during

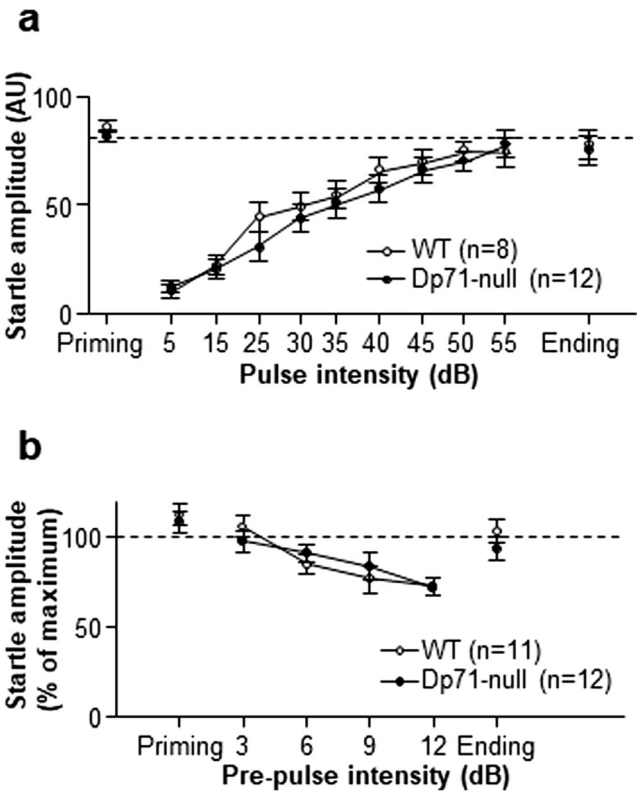

Fig. 4 Gating of auditory stimuli. **a** Startle reflex expressed in arbitrary units as a function of auditory pulse intensity (from 5 to 55 dB above BWN). **b** Prepulse inhibition (PPI) of the acoustic startle reflex expressed as the amplitude of the startle in response to the startling pulse (55 dB) when preceded by a prepulse of 3, 6, 9, or 12 dB above background. Data are normalized to the maximal amplitude recorded in the absence of prepulse. Priming and ending pulses (average of three pulses) were applied at 120 dB (55 dB above background) to verify stability of the maximal startle response before and after application of the pulse ramp. The number of mice per genotype is indicated in each figure part

reversal learning (distance swum, $p < 0.03$; entries in quadrant previously containing platform, $p = 0.05$). This reflected a lack of performance improvement in the Dp71-null mice (both parameters, $p > 0.6$, NS), suggesting inflexible use of non-spatial navigation strategies.

Spatial cognitive flexibility was further assessed in a radial maze using a win-stay paradigm in which only one arm was baited during 10 days of training. Reversal learning was then tested during 4 days during which the bait was moved to a different arm. Mice of both genotypes showed comparable performance during pretraining (latency to visit the first arm, $p > 0.7$; number of arms visited, $p > 0.8$) and latencies of the first visit remained stable throughout the experiment ($p > 0.05$) and comparable in the two genotypes ($p > 0.4$). During training, both genotypes rapidly mastered the task and displayed comparable reference and working memory performance across sessions ($p > 0.3$, Fig. 5c-d). Upon reversal (day 11), the number of reference and working memory errors drastically increased in both genotypes (genotype effect, $p > 0.4$). However, the progression of reference memory performance during reversal learning was significantly delayed in Dp71-null mice compared to WT mice (genotype x session interaction, $p < 0.007$). As shown in Fig. 5c, during the second day of reversal learning, the transgenic mice made more reference memory errors ($p < 0.002$) and more visits of the incorrect arm ($p < 0.02$), suggesting altered spatial cognitive flexibility.

Spatial Working Memory

Working memory performance was first assessed in a low-interference win-shift paradigm (online resource; Fig. S5). During training (7 days, two trials per day), the number of reentries into visited arms during the presentation phase (access to three baited arms) was comparable between genotypes. During the choice phase, the number of visits of non-baited arms (i.e., arms previously explored during the presentation phase) was also comparable between genotypes. When working memory performance was challenged by increasing the delay between the presentation and choice phases to 30 s instead of 15 s (delay test; day 8), no significant difference was detected between genotypes.

In the high-interference delayed non-matching to place task (DNMTP), mice were sequentially submitted to two choice pairs between a recently visited arm and a new adjacent arm (Fig. 5e). During each trial, only the visits to a new arm allowed the mice to retrieve a reward (correct choices). As shown in Fig. 5f, the percentage of correct choices increased across daily sessions in both genotypes (session effect, $p < 0.001$; genotype x session interaction, $p > 0.5$, NS), thus reflecting acquisition of the learning rule. However, the percentage of correct choices was constantly reduced in Dp71-null mice throughout the learning period (genotype effect, $p < 0.003$), suggesting persistent impairment in working memory performance. Figure 5g shows that this deficit was expressed during each choice trial (Genotype effect, first choice, $p < 0.006$; second choice, $p < 0.02$).

Discussion

The major finding of this study is that a genetic loss of Dp71 dystrophin is associated with an excitatory/inhibitory (E/I) imbalance toward enhanced excitation in medial prefrontal cortex (mPFC) neuronal networks, associated with altered executive functions that depend on prefrontal cortex integrity. A role for Dp71 dystrophin in neuronal excitability was suspected because of its major role in clustering AQP4 water channels and Kir4.1 potassium channels in retina and brain perivascular glial endfeet, suggesting that its loss could alter brain water homeostasis and increase extracellular potassium concentration with a putative impact on neuronal firing processes [18, 19, 39–48]. Recent studies support a role of AQP4

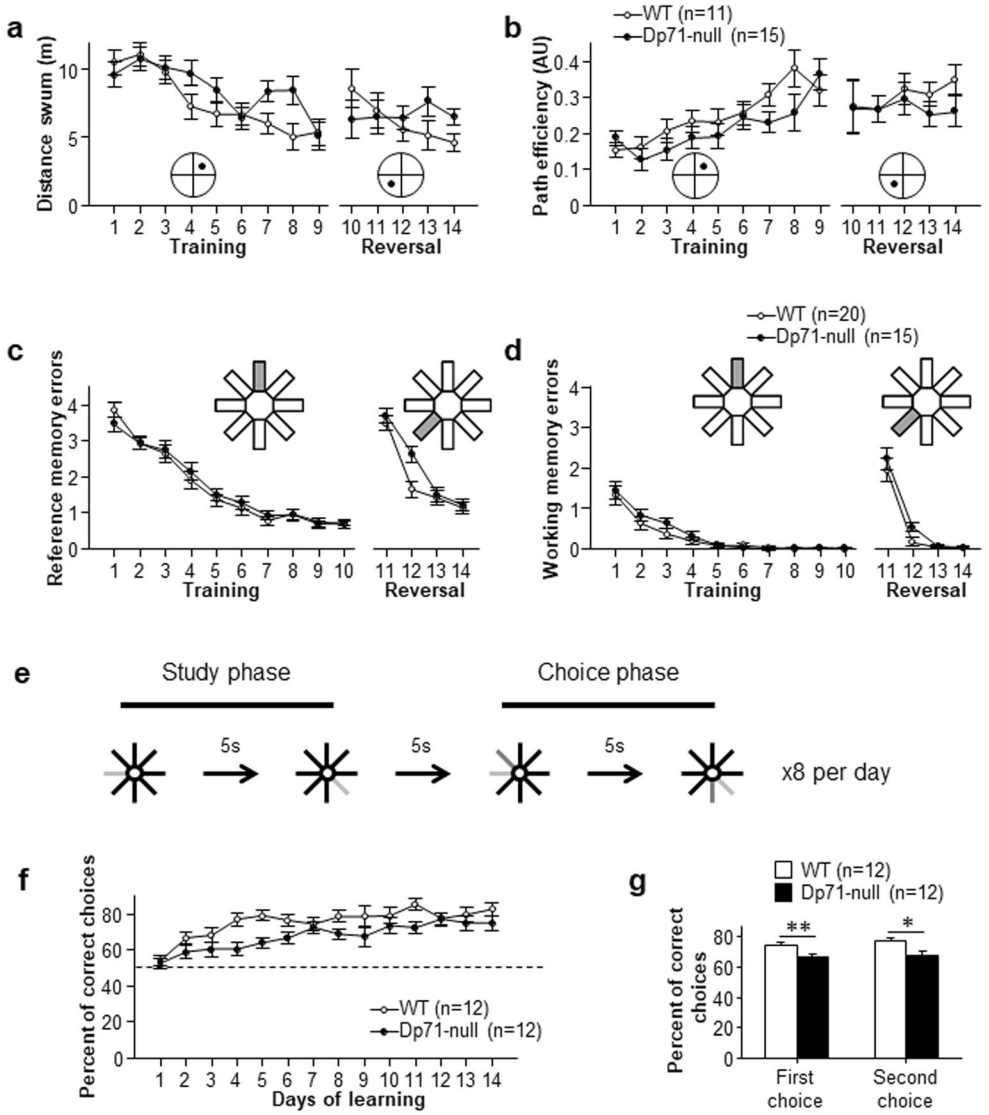

Fig. 5 Spatial cognitive flexibility and working memory. **a–b** Performance during spatial learning (days 1–9) and reversal (days 10–14; platform moved to opposite quadrant as shown in insets) in the water maze task, expressed as distance swum (m) to platform (**a**) and navigation path efficiency (arbitrary unit, AU) (**b**). **c–d** Performance during spatial learning (days 1–10) and reversal (days 11–14; baited arm moved 135° anticlockwise as shown in insets) in the radial-arm maze, expressed as the number of reference memory (**c**) and working memory errors (**d**). **e–g** Delayed non-matching to place. The drawing in **e** shows the protocol composed of a study phase during which mice have sequential access to two arms (light gray arms) with 5-s intervals between trials, followed by a choice phase with sequential access to two sets of arms, including one already visited during the study phase and a new baited arm (dark gray arms). **f** Spatial working memory performance recorded during 14 days expressed as the percentage of correct choices (entering the new baited arm). **g** Mean percentage of correct choices performed during the first or second choice between sets of two arms. $*p < 0.05$, $**p < 0.01$, genotype effect. The number of mice per genotype is indicated in each figure part

and Kir4.1 channels in synaptic plasticity and cognitive processes and their implication in several neurodegenerative and neurodevelopmental diseases [49–55], suggesting that glial pathophysiological mechanisms could mainly underlie the cognitive impairment associated with Dp71 loss. However, Dp71 has also been detected in neurons [56, 57] and in postsynaptic densities [20, 58], and an alternative transcript called Dp40 has been proposed to play a role in presynaptic and/or postsynaptic mechanisms in central excitatory synapses [59, 60]. In addition to its major role in glial mechanisms, Dp71 may thus directly contribute to synapse function and Dp71 loss may therefore induce complex and multifactorial brain alterations. The present study suggests that altered E/I balance, neurotransmission, and synaptic plasticity of cortical networks involved in cognitive and executive processes are major deteriorated systems likely contributing to the genesis of intellectual disability in DMD patients lacking Dp71.

Cortical synaptic E/I balance results from coordinated and regulated activities of recurrent excitatory and inhibitory cortical networks. The E/I balance is normally finely tuned to a 20–80%

set point in rodents and small shifts may have important impact on neuronal network activity [30, 61–63]. Here, we report an 8% increase in excitation in Dp71-null mice, corresponding to 46% increase of the E/I ratio. This is associated with a strong enhancement of basal excitatory current amplitudes and significant reduction of the level of synaptic plasticity (LTP) in prefrontal cortical networks. This change could not be attributed to any modification of neuron membrane passive properties. In contrast, we found that Dp71 loss selectively alters the AMPA receptor-mediated component of fast glutamatergic transmission in mPFC; whereas, NMDA-receptor currents are not significantly modified. Amplitude and frequency of spontaneous miniature inhibitory currents were unaltered, indicating that the loss of Dp71 has no major impact on GABA release mechanisms and GABA receptor properties. The frequency of miniature excitatory events was reduced in Dp71-null mice. This suggests a reduced probability of presynaptic glutamate release that may result from a reduced number of functional glutamatergic synapses and/or alterations in presynaptic ultrastructure and glutamate release mechanisms as suggested earlier [20, 21, 59]. But this cannot explain the enhanced excitation observed in these mice. In contrast, we demonstrate here that the amplitude of postsynaptic AMPA-receptor currents is significantly increased in Dp71-null mice, as well as the amplitude of miniature excitatory currents. Thus, postsynaptic alterations, such as changes in postsynaptic AMPA-receptor density, may likely contribute to enhanced excitation in these mice. The decay time constant of AMPAr-mediated mEPSC is reduced in Dp71-null mice, suggesting changes in AMPA-receptor properties and/or subunit composition [64, 65]. Presence of larger clusters of the postsynaptic protein PSD-95 in confocal image analyses also favors a main postsynaptic hypothesis [66].

Long-term potentiation (LTP) of mPFC synaptic transmission was significantly reduced in principal neurons of Dp71-null mice. LTP of the AMPA-receptor component of neurotransmission was significantly reduced, while that of inhibitory inputs was not significantly altered. In contrast, paired-pulse facilitation, a short-lasting form of plasticity mediated in part by presynaptic mechanisms [67], was unaffected. We suggest that Dp71 loss-induced structural changes during neuronal network development, such as abnormal architectural structuring of synaptic connections within excitatory microcircuits and putative changes in excitatory synapse molecular organization and morphology [20, 21], leading to enhanced neuronal excitability and modification of the set point of the balance between excitatory and inhibitory inputs. If the large enhancement of excitatory transmission relies on altered AMPA-receptor density, the reduced magnitude of LTP might result from a reduced capacity for fast mobilization of a more important number of these receptors to stabilize synaptic strengthening during plasticity.

Synaptic plasticity and E/I balance are critical factors for fine tuning of neuronal circuits, networks oscillations, and homeostatic plasticity [68, 69], and an elevation of the E/I ratio in mPFC was reported as a contributing pathophysiological factor in neurodevelopmental disorders associated with executive dysfunction [13–15]. We therefore addressed whether the neurophysiological defects evidenced here in mPFC networks of Dp71-null mice could be linked to executive processing disabilities. We first showed that Dp71-null mice have no deficit when tested for prepulse inhibition (PPI) of the acoustic startle reflex, a translational paradigm frequently used to detect deficits in gating sensorimotor inputs or early attentional control in rodent models of neuropsychiatric disorders [70]. In contrast, we found that Dp71-null mice may display altered executive functions such as spatial cognitive flexibility and working memory: In a win-stay paradigm in an automated radial maze with doors, initial learning, and reference memory errors were unaffected, but their capacity to adapt exploration strategies during reversal learning was delayed. No such deficits were detected in Dp427-deficient *mdx* mice [23], suggesting that impaired spatial cognitive flexibility is selectively associated with genetic loss of the Dp71 product of the *dmd* gene. We also investigated spatial working memory performance in win-shift paradigms in the radial maze, in which newly acquired information needs to be updated on a moment-to-moment basis to guide adapted behavior. In a simple low-interference task, in which mice had to remember the spatial position of three visited arms in order to avoid errors during a subsequent choice trial, mice of both genotypes displayed comparable performance, indicating that they were able to learn the rule and integrate cues and contingencies required for spatial learning tasks. Increasing the delay between the presentation and choice phases did not alter performance, suggesting that the two genotypes display comparable capacity to retain information in short-term memory storage to complete a directed task. In contrast, Dp71-null mice displayed a persistent performance deficit in the delayed non-matching to place paradigm. In this high-interference task, intertrial delays were short (5 s), but mice needed to maintain information in spite of competing demand and task-relevant proactive and retroactive interferences in a series of successive choice trials. In both humans and rodents, general cognitive or intellectual abilities are strongly associated with the processing component of working memory, which requires resistance to interference and depends on prefrontal cortex, while the capacity for short-term maintenance of information is a poor predictor of cognitive level [12]. The selective deficit shown by Dp71-null mice in the high-interference working memory task suggests alterations in the critical functions required to learn associations between temporally contingent stimuli and to cope with changing environments. This is a relevant phenotype analogous to the endophenotype

thought to underlie individual differences in intellectual abilities in the human condition.

Conclusions

Altered glutamatergic synapse function leading to enhanced excitation appears as a main and reliable outcome in the Dp71-deficient brain. The enhanced excitation and reduced synaptic plasticity in mPFC neuronal network is associated with selective impairments in the processing component of spatial working memory and cognitive flexibility. Our results suggest that elevated cellular excitation in prefrontal networks perturbs executive processes, which are viewed as critical for intellectual functioning in humans. This is also in line with neurobehavioral models pointing to E/I imbalance and executive dysfunctions as key pathophysiological factor in neurodevelopmental diseases with comorbid diagnosis of intellectual disability and neuropsychiatric disorders. Although intellectual disability in DMD may also occur with the loss of other brain dystrophins, particularly Dp140, it is noteworthy that a strong association was found between Dp71 loss and the deterioration of working memory in DMD patients with mutations downstream of exon 63 [10]. As such mutations at the 3′ end of the gene increase the risk for comorbid diagnosis of neuropsychiatric disorders such as autism, it will be important in future studies to determine whether Dp71 loss favors social behavior deficits. A recent case study reporting a selective dysfunction of Dp71 associated with intellectual disability without myopathy [7] further supports the relevance of the Dp71-null mouse to unravel the mechanisms of intellectual disability in DMD. The present study provides new insights on the neurophysiological mechanisms and cognitive processes altered when Dp71 is missing, which may also suggest new directions for therapeutic developments targeting excitatory neurotransmission, as well as for guidance of academic environment in this severely affected subpopulation of DMD children.

Acknowledgements We are grateful to the Zootechnic platform of our institute for mouse breeding, care, and genotyping and to Glenn Dallérac for the advice in electrophysiology.

Funding This work was supported by Centre National de la Recherche Scientifique (CNRS, France) and University Paris-Sud (France), and by grants from Association Française contre les Myopathies (AFM, France; grant number 15299) and Agence Nationale de la Recherche (ANR, France; grant number ANR-14-CE13-0037-01) to C.V. and by a PhD fellowship from Ministère de l'Enseignement Supérieur et de la Recherche (France) to R.C.

Compliance with Ethic Standards

Experiments involving animals were undertaken following the guidelines of the European Directive 2010/63/EU, French National Committee (87/848), and local mouse facility (agreement #D91–471-104), with official approval (#2635) from the CEEA59 ethical committee (Comité d'éthique en matière d'expérimentation animale Paris Centre et Sud) and Ministère de l'Enseignement Supérieur et de la Recherche (France).

Conflict of Interest The authors declare they have no conflict of interest.

References

1. Lenk U, Hanke R, Thiele H, Speer A (1993) Point mutations at the carboxy terminus of the human dystrophin gene: implications for an association with mental retardation in DMD patients. Hum Mol Genet 2:1877–1881
2. Desguerre I, Christov C, Mayer M, Zeller R, Becane HM, Bastuji-Garin S, Leturcq F, Chiron C et al (2009) Clinical heterogeneity of Duchenne muscular dystrophy (DMD): definition of sub-phenotypes and predictive criteria by long-term follow-up. PLoS One 4:e4347
3. Taylor PJ, Betts GA, Maroulis S, Gilissen C, Pedersen RL, Mowat DR, Johnston HM, Buckley MF (2010) Dystrophin gene mutation location and the risk of cognitive impairment in Duchenne muscular dystrophy. PLoS One 5:e8803
4. Milic Rasic V, Vojinovic D, Pesovic J, Mijalkovic G, Lukic V, Mladenovic J, Kosac A, Novakovic I et al (2015) Intellectual ability in the Duchenne muscular dystrophy and dystrophin gene mutation location. Balkan J Med Genet 17:25–35
5. Moizard MP, Toutain A, Fournier D, Berret F, Raynaud M, Billard C, Andres C, Moraine C (2000) Severe cognitive impairment in DMD: obvious clinical indication for Dp71 isoform point mutation screening. Eur J Hum Genet 8:552–556
6. Daoud F, Angeard N, Demerre B, Martie I, Benyaou R, Leturcq F, Cossée M, Deburgrave N et al (2009a) Analysis of Dp71 contribution in the severity of mental retardation through comparison of Duchenne and Becker patients differing by mutation consequences on Dp71 expression. Hum Mol Genet 18:3779–3794
7. De Brouwer AP, Nabuurs SB, Verhaart IE, Oudakker AR, Hordijk R, Yntema HG, Hordijk-Hos JM, Voesenek K et al (2014) A 3-base pair deletion, c.9711_9713del, in DMD results in intellectual disability without muscular dystrophy. Eur J Hum Genet 22:480–485
8. Snow WM, Anderson JE, Jakobson LS (2013) Neuropsychological and neurobehavioral functioning in Duchenne muscular dystrophy: A review. Neurosci Biobehav Rev 37:743–752
9. Mento G, Tarantino V, Bisiacchi PS (2011) The neuropsychological profile of infantile Duchenne muscular dystrophy. Clin Neuropsychol 25:1359–1377
10. Ricotti V, Mandy WP, Scoto M, Pane M, Deconinck N, Messina S, Mercuri E, Skuse DH et al (2016) Neurodevelopmental, emotional, and behavioural problems in Duchenne muscular dystrophy in relation to underlying dystrophin gene mutations. Dev Med Child Neurol 58:77–84
11. Jones MW (2002) A comparative review of rodent prefrontal cortex and working memory. Curr Mol Med 2:639–647
12. Matzel LD, Kolata S (2010) Selective attention, working memory, and animal intelligence. Neurosci Biobehav Rev 34:23–30
13. Gatto CL, Broadie K (2010) Genetic controls balancing excitatory and inhibitory synaptogenesis in neurodevelopmental disorder models. Front Synaptic Neurosci 2:4
14. Vinkers CH, Mirza NR, Olivier B, Kahn RS (2010) The inhibitory GABA system as a therapeutic target for cognitive symptoms in schizophrenia: investigational agents in the pipeline. Expert Opin Investig Drugs 19:1217–1233
15. Yizhar O, Fenno LE, Prigge M, Schneider F, Davidson TJ, O'Shea DJ, Sohal VS, Goshen I et al (2011) Neocortical excitation/inhibition balance in information processing and social dysfunction. Nature 477:171–178

16. Lederfein D, Levy Z, Augier N, Mornet D, Morris G, Fuchs O, Yaffe D, Nudel U (1992) A 71-kilodalton protein is a major product of the Duchenne muscular dystrophy gene in brain and other nonmuscle tissues. Proc Natl Acad Sci U S A 89:5346–5350
17. Waite A, Brown SC, Blake DJ (2012) The dystrophin-glycoprotein complex in brain development and disease. Trends Neurosci 35: 487–496
18. Tadayoni R, Rendon A, Soria-Jasso LE, Cisneros B (2012) Dystrophin Dp71: the smallest but multifunctional product of the Duchenne muscular dystrophy gene. Mol Neurobiol 45: 43–60
19. Hendriksen RG, Hoogland G, Schipper S, Hendriksen JG, Vles JS, Aalbers MW (2015) A possible role of dystrophin in neuronal excitability: a review of the current literature. Neurosci Biobehav Rev 51:255–262
20. Daoud F, Candelario-Martínez A, Billard JM, Avital A, Khelfaoui M, Rozenvald Y, Guegan M, Mornet D et al (2009b) Role of mental retardation-associated dystrophin-gene product Dp71 in excitatory synapse organization, synaptic plasticity and behavioral functions. PLoS One 4:e6574
21. Miranda R, Nudel U, Laroche S, Vaillend C (2011) Altered presynaptic ultrastructure in excitatory hippocampal synapses of mice lacking dystrophins Dp427 or Dp71. Neurobiol Dis 43:134–141
22. Sarig R, Mezger-Lallemand V, Gitelman I, Davis C, Fuchs O, Yaffe D, Nudel U (1999) Targeted inactivation of Dp71, the major non-muscle product of the DMD gene: differential activity of the Dp71 promoter during development. Hum Mol Genet 8:1–10
23. Chaussenot R, Edeline JM, Le Bec B, El Massioui N, Laroche S, Vaillend C (2015) Cognitive dysfunction in the dystrophin-deficient mouse model of Duchenne muscular dystrophy: a reappraisal from sensory to executive processes. Neurobiol Learn Mem 124:111–122
24. Paxinos G, Franklin KBJ (2001) The mouse brain in stereotaxic coordinates, 2nd edn. Academic Press, San Diego
25. Vaillend C, Perronnet C, Ros C, Gruszczynski C, Goyenvalle A, Laroche S, Danos O, Garcia L et al (2010) Rescue of a dystrophin-like protein by exon skipping in vivo restores GABAA-receptor clustering in the hippocampus of the mdx mouse. Mol Ther 18: 1683–1688
26. Borg-Graham LJ, Monier C, Frégnac Y (1998) Visual input evokes transient and strong shunting inhibition in visual cortical neurons. Nature 393:369–373
27. Monier C, Chavane F, Baudot P, Graham LJ, Frégnac Y (2003) Orientation and direction selectivity of synaptic inputs in visual cortical neurons: a diversity of combinations produces spike tuning. Neuron 37:663–680
28. Moreau AW, Amar M, Le Roux N, Morel N, Fossier P (2010) Serotoninergic fine-tuning of the excitation-inhibition balance in rat visual cortical networks. Cereb Cortex 20:456–467
29. Meunier CN, Callebert J, Cancela JM, Fossier P (2015) Effect of dopaminergic D1 receptors on plasticity is dependent of serotoninergic 5-HT1A receptors in L5-pyramidal neurons of the prefrontal cortex. PLoS One 10:e0120286
30. Le Roux N, Amar M, Baux G, Fossier P (2006) Homeostatic control of the excitation-inhibition balance in cortical layer 5 pyramidal neurons. Eur J Neurosci 24:3507–3718
31. Haider B, Duque A, Hasenstaub AR, McCormick DA (2006) Neocortical network activity in vivo is generated through a dynamic balance of excitation and inhibition. J Neurosci 26:4535–4545
32. Higley MJ, Contreras D (2006) Balanced excitation and inhibition determine spike timing during frequency adaptation. J Neurosci 26: 448–457
33. Abraham WC, Huggett A (1997) Induction and reversal of long-term potentiation by repeated high-frequency stimulation in rat hippocampal slices. Hippocampus 7:137–145
34. Touzani K, Puthanveettil SV, Kandel ER (2007) Consolidation of learning strategies during spatial working memory task requires protein synthesis in the prefrontal cortex. Proc Natl Acad Sci U S A 104:5632–5637
35. McCormick DA, Connors BW, Lighthall JW, Prince DA (1985) Comparative electrophysiology of pyramidal and sparsely spiny stellate neurons of the neocortex. J Neurophysiol 54:782–806
36. Connors BW, Gutnick MJ (1990) Intrinsic firing patterns of diverse neocortical neurons. Trends Neurosci 13:99–104
37. Zucker RS, Regehr WG (2002) Short-term synaptic plasticity. Annu Rev Physiol 64:355–405
38. Katz B, Miledi R (1968) The role of calcium in neuromuscular facilitation. J Physiol 195:481–492
39. Connors NC, Kofuji P (2002) Dystrophin Dp71 is critical for the clustered localization of potassium channels in retinal glial cells. J Neurosci 22(11):4321–4327
40. Dalloz C, Sarig R, Fort P, Yaffe D, Bordais A, Pannicke T, Grosche J, Mornet D et al (2003) Targeted inactivation of dystrophin gene product Dp71: phenotypic impact in mouse retina. Hum Mol Genet 12(13):1543–1554
41. Fort PE, Sene A, Pannicke T, Roux MJ, Forster V, Mornet D, Nudel U, Yaffe D et al (2008) Kir4.1 and AQP4 associate with Dp71- and utrophin-DAPs complexes in specific and defined microdomains of Müller retinal glial cell membrane. Glia 56(6):597–610
42. Nicchia GP, Rossi A, Nudel U, Svelto M, Frigeri A (2008) Dystrophin-dependent and -independent AQP4 pools are expressed in the mouse brain. Glia 56(8):869–876
43. Sene A, Tadayoni R, Pannicke T, Wurm A, El Mathari B, Benard R, Roux MJ, Yaffe D et al (2009) Functional implication of Dp71 in osmoregulation and vascular permeability of the retina. PLoS One 4(10):e7329
44. Cia D, Simonutti M, Fort PE, Doly M, Rendon A (2014) Slight alteration of the electroretinogram in mice lacking dystrophin dp71. Ophthalmic Res 51(4):196–203
45. Vacca O, Darche M, Schaffer DV, Flannery JG, Sahel JA, Rendon A, Dalkara D (2014) AAV-mediated gene delivery in Dp71-null mouse model with compromised barriers. Glia 62(3):468–476
46. Vacca O, Charles-Messance H, El Mathari B, Sene A, Barbe P, Fouquet S, Aragón J, Darche M et al (2016) AAV-mediated gene therapy in dystrophin-Dp71 deficient mouse leads to blood-retinal barrier restoration and oedema reabsorption. Hum Mol Genet 25(14):3070–3079
47. De Bellis M, Pisani F, Mola MG, Rosito S, Simone L, Buccoliero C, Trojano M, Nicchia GP et al (2017) Translational readthrough generates new astrocyte AQP4 isoforms that modulate supramolecular clustering, glial endfeet localization, and water transport. Glia 65(5):790–803
48. Helleringer R, Le Verger D, Li X, Izabelle C, Chaussenot R, Belmaati-Cherkaoui M, Dammak R, Decottignies P, Daniel H, Galante M, Vaillend C (2018) Cerebellar synapse properties and cerebellum-dependent motor and non-motor performance in Dp71-null mice. Dis Model Mech 11(7).
49. Sicca F, Imbrici P, D'Adamo MC, Moro F, Bonatti F, Brovedani P, Grottesi A, Guerrini R et al (2011) Autism with seizures and intellectual disability: possible causative role of gain-of-function of the inwardly-rectifying K+ channel Kir4.1. Neurobiol Dis 43(1):239–247
50. Skucas VA, Mathews IB, Yang J, Cheng Q, Treister A, Duffy AM, Verkman AS, Hempstead BL et al (2011) Impairment of select forms of spatial memory and neurotrophin-dependent synaptic plasticity by deletion of glial aquaporin-4. J Neurosci 31(17):6392–6397
51. Scharfman HE, Binder DK (2013) Aquaporin-4 water channels and synaptic plasticity in the hippocampus. Neurochem Int 63(7):702–711
52. Sibille J, Pannasch U, Rouach N (2014) Astroglial potassium clearance contributes to short-term plasticity of synaptically evoked currents at the tripartite synapse. J Physiol 592(1):87–102

53. Nwaobi SE, Cuddapah VA, Patterson KC, Randolph AC, Olsen ML (2016) The role of glial-specific Kir4.1 in normal and pathological states of the CNS. Acta Neuropathol 132(1):1–21
54. Hubbard JA, Szu JI, Binder DK (2018) The role of aquaporin-4 in synaptic plasticity, memory and disease. Brain Res Bull 136:118–129
55. Woo J, Kim JE, Im JJ, Lee J, Jeong HS, Park S, Jung SY, An H et al (2018) Astrocytic water channel aquaporin-4 modulates brain plasticity in both mice and humans: a potential gliogenetic mechanism underlying language-associated learning. Mol Psychiatry 23(4): 1021–1030
56. Gorecki DC, Barnard EA (1995) Specific expression of G-dystrophin (Dp71) in the brain. Neuroreport 6:893–896
57. Aleman V, Osorio B, Chavez O, Rendon A, Mornet D, Martinez D (2001) Subcellular localization of Dp71 dystrophin isoforms in cultured hippocampal neurons and forebrain astrocytes. Histochem Cell Biol 115:243–254
58. Blake DJ, Hawkes R, Benson MA, Beesley PW (1999) Different dystrophin-like complexes are expressed in neurons and glia. J Cell Biol 147:645–658
59. Tozawa T, Itoh K, Yaoi T, Tando S, Umekage M, Dai H, Hosoi H, Fushiki S (2012) The shortest isoform of dystrophin (Dp40) interacts with a group of presynaptic proteins to form a presumptive novel complex in the mouse brain. Mol Neurobiol 45:287–297
60. Fujimoto T, Itoh K, Yaoi T, Fushiki S (2014) Somatodendritic and excitatory postsynaptic distribution of neuron-type dystrophin isoform, Dp40, in hippocampal neurons. Biochem Biophys Res Commun 452:79–84
61. Le Roux N, Amar M, Moreau A, Fossier P (2007) Involvement of NR2A- or NR2B-containing N-methyl-D-aspartate receptors in the potentiation of cortical layer 5 pyramidal neurone inputs depends on the developmental stage. Eur J Neurosci 26:289–301
62. Le Roux N, Amar M, Moreaux A, Fossier P (2008) Impaired GABAergic transmission disrupts normal homeostatic plasticity in rat cortical networks. Eur J Neurosci 27:3244–3256
63. Meunier C, Amar M, Lanfumey L, Hamon M, Fossier P (2013) 5-HT(1A) receptors direct the orientation of plasticity in layer 5 pyramidal neurons of the mouse prefrontal cortex. Neuropharm 71: 37–45
64. Greger IH, Ziff EB, Penn AC (2007) Molecular determinants of AMPA receptor subunit assembly. Trends Neurosci 30:407–416
65. Howe JR (2015) Modulation of non-NMDA receptor gating by auxiliary subunits. J Physiol 593:61–72
66. Losi G, Prybylowski K, Fu Z, Luo J, Wenthold RJ, Vicini S (2003) PSD-95 regulates NMDA receptors in developing cerebellar granule neurons of the rat. J Physiol 548:21–29
67. Thomson AM (2000) Facilitation, augmentation and potentiation at central synapses. Trends Neurosci 23:305–312
68. Fritschy JM (2008) Epilepsy, E/I balance and GABA(a) receptor plasticity. Front Mol Neurosci 1:5
69. Pozo K, Goda Y (2010) Unraveling mechanisms of homeostatic synaptic plasticity. Neuron 66:337–351
70. Kohl S, Heekeren K, Klosterkötter J, Kuhn J (2013) Prepulse inhibition in psychiatric disorders–apart from schizophrenia. J Psychiatr Res 47:445–452